

A UNIFIED DIFFUSION BRIDGE FRAMEWORK VIA STOCHASTIC OPTIMAL CONTROL

Kaizhen Zhu^{1*}, Mokai Pan^{1*}, Yuexin Ma¹, Yanwei Fu², Jingyi Yu¹, Jingya Wang¹, Ye Shi^{1†}

¹MoE Key Laboratory of Intelligent Perception and Human-Machine Collaboration, ShanghaiTech University

²Fudan University

{zhukzh2024, panmk, mayuexin}@shanghaitech.edu.cn

{yanweifu}@fudan.edu.cn

{yujingyi, wangjingya, shiye}@shanghaitech.edu.cn

ABSTRACT

Recent advances in diffusion bridge models leverage Doob’s h -transform to establish fixed endpoints between distributions, demonstrating promising results in image translation and restoration tasks. However, these approaches frequently produce blurred or excessively smoothed image details and lack a comprehensive theoretical foundation to explain these shortcomings. To address these limitations, we propose a **Unified** framework for **Diffusion Bridges** (UniDB) based on Stochastic Optimal Control (SOC). UniDB formulates the problem through an SOC-based optimization and derives a closed-form solution for the optimal controller, thereby unifying and generalizing existing diffusion bridge models. We demonstrate that existing diffusion bridges employing Doob’s h -transform constitute a special case of our framework, emerging when the terminal penalty coefficient in the SOC cost function tends to infinity. By incorporating a tunable terminal penalty coefficient, UniDB achieves an optimal balance between control costs and terminal penalties, substantially improving detail preservation and output quality. Notably, UniDB seamlessly integrates with existing diffusion bridge models, requiring only minimal code modifications. Extensive experiments across diverse image restoration tasks validate the superiority and adaptability of the proposed framework. Our code is available at <https://github.com/UniDB-SOC/UniDB/>.

1 INTRODUCTION

The diffusion model has been extensively utilized across a range of applications, including image generation and editing Ho et al. (2020); Kawar et al. (2022); Song et al. (2020); Xia et al. (2023); Li et al. (2023), imitation learning Wu et al. (2024); Chi et al. (2023); Ze et al. (2024) and reinforcement learning Yang et al. (2023); Ding et al. (2024a), etc. Despite its versatility, the standard diffusion model faces limitations in transitioning between arbitrary distributions due to its inherent assumption of a Gaussian noise prior. To overcome this problem, diffusion models Dhariwal & Nichol (2021); Ho & Salimans (2022); Murata et al. (2023); Ding et al. (2024b); Chung et al. (2022); Tang et al. (2024) often rely on meticulously designed conditioning mechanisms and classifier/loss guidance to facilitate conditional sampling and ensure output alignment with a target distribution. However, these methods can be cumbersome and may introduce manifold deviations during the sampling process. Meanwhile, Diffusion Schrödinger Bridge Shi et al. (2024); De Bortoli et al. (2021); Somnath et al. (2023) involves constraints that hinder direct optimization of the KL divergence, resulting in slow convergence and limited model fitting capability.

To address this challenge, DDBMs Zheng et al. (2024) proposed a diffusion bridge model using Doob’s h -transform. This framework is specifically designed to establish fixed endpoints between two distinct distributions by learning the score function of the diffusion bridge from data, and then solving the stochastic differential equation (SDE) based on these learned scores to transition from one

*Equal contribution.

†Correspondence to: Ye Shi <shiye@shanghaitech.edu.cn>.

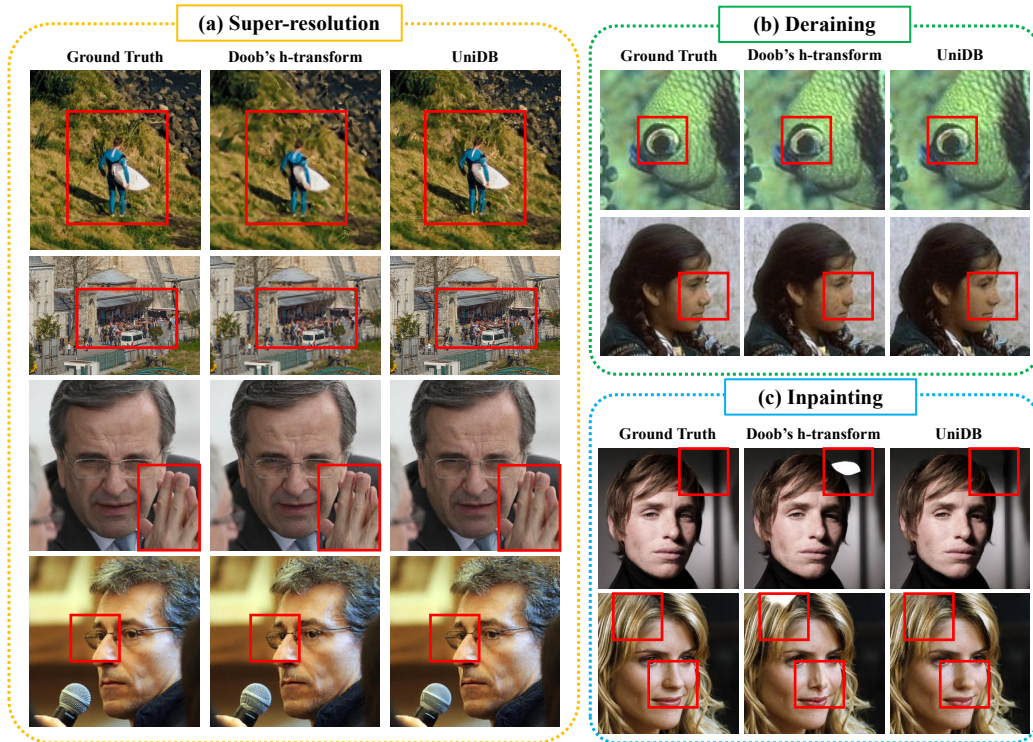


Figure 1: Here we briefly compare the performance of UniDB to diffusion bridge with Doob’s h -transform Yue et al. (2023) across various tasks, including Super-resolution, Inpainting and Deraining. UniDB effectively balances control and terminal costs by modifying the terminal penalty coefficient, alleviating the problems caused by Doob’s h -transform in these applications. This framework significantly boosts the detail rendering ability of generated images while imposing minimal overhead in code modifications.

endpoint distribution to another. However, the forward SDE in DDBMs lacks the mean information of the terminal distribution, which restricts the quality of the generated images, particularly in image restoration tasks. Subsequently, GOUB Yue et al. (2023) extends this framework by integrating Doob’s h -transform with a mean-reverting SDE, achieving better results compared to DDBMs. Despite the promising results in diffusion bridge with Doob’s h -transform, two fundamental challenges persist: 1) the theoretical mechanisms by which Doob’s h -transform governs the bridging process remain poorly understood, lacking a rigorous framework to unify its empirical success; and 2) while effective for global distribution alignment, existing methods frequently degrade high-frequency details—such as sharp edges and fine textures—resulting in outputs with blurred or oversmoothed artifacts that compromise perceptual fidelity. These limitations underscore the need for both theoretical grounding and enhanced detail preservation in diffusion bridges.

In this paper, we revisit the diffusion bridges through the lens of stochastic optimal control (SOC) by introducing a novel framework called UniDB, which formulates an optimization problem based on SOC principles to implement diffusion bridges. It enables the derivation of a closed-form solution for the optimal controller, along with the corresponding training objective for the diffusion bridge. UniDB identifies Doob’s h -transform as a special case when the terminal penalty coefficient in the SOC cost function approaches infinity. This explains why Doob’s h -transform may result in suboptimal solutions with blurred or distorted details. To address this limitation, UniDB utilizes the penalty coefficient in SOC to adjust the expressiveness of the image details and enhance the authenticity of the generated outputs. Our main contributions are as follows:

- We introduce UniDB, a novel unified diffusion bridge framework based on stochastic optimal control. This framework generalizes existing diffusion bridge models like DDBMs and GOUB, offering a comprehensive understanding and extension of Doob’s h -transform by incorporating general forward SDE forms.

- We derive closed-form solutions for the SOC problem, demonstrating that Doob’s h -transform is merely a special case within UniDB when the terminal penalty coefficient in the SOC cost function approaches infinity. This insight reveals inherent limitations in the existing diffusion bridge approaches, which UniDB overcomes. Notably, the improvement of UniDB requires minimal code modification, ensuring easy implementation.
- UniDB achieves state-of-the-art results in various image restoration tasks, including super-resolution (DIV2K), inpainting (CelebA-HQ), and deraining (Rain100H), which highlights the framework’s superior image quality and adaptability across diverse scenarios.

2 RELATED WORK

Diffusion with Guidance. This technique tackles conditional generative tasks by leveraging a differentiable loss function for guidance without the need for additional training Chung et al. (2022); Shenoy et al. (2024); Bradley & Nakkiran (2024). However, it often yields suboptimal image quality and a prolonged sampling process due to the necessity of small step sizes. Most importantly, the sampling process is prone to manifold deviations and detail losses Yang et al. (2024). Furthermore, enhancing the guidance of the diffusion typically requires the introduction of additional modules, thereby increasing the model’s computational complexity.

Diffusion Bridge with Doob’s h -transform. Recent advances in diffusion bridging have demonstrated the efficacy of Doob’s h -transform in enhancing transition quality between arbitrary distributions. Notably, DDBMs Zhou et al. (2023) pioneered this approach by employing a linear SDE combined with Doob’s h -transform to construct direct diffusion bridges. Subsequently, GOUB Yue et al. (2023) extends this framework by integrating Doob’s h -transform with a mean-reverting SDE, achieving state-of-the-art performance in image restoration tasks. Despite these empirical successes, the theoretical foundations of Doob’s h -transform in this context remain insufficiently explored. In addition, these methods often result in images with blurred or oversmoothed features, particularly affecting the capture of high-frequency details crucial for perceptual fidelity.

Diffusion with Stochastic Optimal Control. The integration of SOC principles into diffusion models has emerged as a promising paradigm for guiding distribution transitions. DIS Berner et al. (2022) established a foundational theoretical linkage between diffusion processes and SOC, while RB-Modulation Rout et al. (2024) operationalized SOC via a simplified SDE structure for training-free style transfer using pre-trained diffusion models. Close to our work, DBFS Park et al. (2024) leveraged SOC to construct diffusion bridges in infinite-dimensional function spaces and also established equivalence between SOC and Doob’s h -transform. However, DBFS primarily extends Doob’s h -transform to infinite Hilbert spaces via SOC, without addressing its intrinsic limitations. Our analysis reveals a critical insight: Doob’s h -transform corresponds to a suboptimal solution that can inherently lead to artifacts such as blurred or distorted details. To resolve this, we introduce a unified SOC framework that jointly optimizes trajectory costs and terminal constraints, enhancing detail preservation and image quality.

3 PRELIMINARIES

3.1 DENOISING DIFFUSION BRIDGE MODELS

Starting with an initial d -dimensional data distribution $\mathbf{x}_0 \sim q_{\text{data}}(\mathbf{x})$, diffusion models Song et al. (2020); Ho et al. (2020); Sohl-Dickstein et al. (2015); Song & Ermon (2019) construct a diffusion process, which can be achieved by defining a forward stochastic process evolving from \mathbf{x}_0 and promise the transition probability $p(\mathbf{x}_t | \mathbf{x}_s)$ remains Gaussian Zheng et al. (2024) through a stochastic differential equation (SDE):

$$d\mathbf{x}_t = \mathbf{f}(\mathbf{x}_t, t)dt + g_t d\mathbf{w}_t, \mathbf{f}(\mathbf{x}_t, t) = f(t)\mathbf{x}_t. \quad (1)$$

where t ranges over the interval $[0, T]$, $f(t)$ is some scalar-valued function, $g : [0, T] \rightarrow \mathbb{R}$ signifies the scalar-valued diffusion coefficient and $\mathbf{w}_t \in \mathbb{R}^d$ is the Wiener process, also known as Brownian motion. To realize transition between arbitrary distributions, DDBMs introduces Doob’s h -transform Särkkä & Solin (2019), a mathematical technique applied to stochastic processes, which rectifies the drift term of the forward diffusion process to pass through a preset terminal point $\mathbf{x}_T \in \mathbb{R}^d$. Precisely, the forward process of diffusion bridges after Doob’s h -transform becomes:

$$d\mathbf{x}_t = [\mathbf{f}(\mathbf{x}_t, t) + g_t^2 \mathbf{h}(\mathbf{x}_t, t, \mathbf{x}_T, T)] dt + g_t d\mathbf{w}_t, \quad (2)$$

where $\mathbf{h}(\mathbf{x}_t, t, \mathbf{x}_T, T) = \nabla_{\mathbf{x}_t} \log p(\mathbf{x}_T | \mathbf{x}_t)$ is the h function. The diffusion bridge can connect the initial \mathbf{x}_0 to any given terminal \mathbf{x}_T and thus is promising for various image restoration tasks. Meanwhile, its backward reverse SDE Anderson (1982) is given by

$$d\mathbf{x}_t = \left[\mathbf{f}(\mathbf{x}_t, t) + g_t^2 \nabla_{\mathbf{x}_t} \log p(\mathbf{x}_T | \mathbf{x}_t) - g_t^2 \nabla_{\mathbf{x}_t} \log p(\mathbf{x}_t | \mathbf{x}_T) \right] dt + g_t d\tilde{\mathbf{w}}_t. \quad (3)$$

where $\tilde{\mathbf{w}}_t$ is the reverse-time Wiener process and the unknown term $\nabla_{\mathbf{x}_t} \log p(\mathbf{x}_t | \mathbf{x}_T)$ can be estimated by a score prediction neural network s_θ Song et al. (2020).

3.2 GENERALIZED ORNSTEIN-UHLENBECK BRIDGE

Generalized Ornstein-Uhlenbeck (GOU) process describes a mean-reverting stochastic process commonly used in finance, physics, and other fields in the following SDE form Ahmad (1988):

$$d\mathbf{x}_t = \theta_t (\boldsymbol{\mu} - \mathbf{x}_t) dt + g_t d\mathbf{w}_t, \quad (4)$$

where $\boldsymbol{\mu}$ is a given state vector, θ_t denotes a scalar drift coefficient and g_t represents the diffusion coefficient with θ_t, g_t satisfying the specified relationship $g_t^2 = 2\lambda^2\theta_t$ where λ^2 is a given constant scalar. Based on this, Generalized Ornstein-Uhlenbeck Bridge (GOUB) is a diffusion bridge model Yue et al. (2023), which can address image restoration tasks without the need for specific prior knowledge. With the introduction of $\boldsymbol{\mu}$, \mathbf{x}_t tends to $\boldsymbol{\mu}$ as time t progresses. Through Doob's h -transform, denote $\bar{\theta}_{s:t} = \int_s^t \theta_z dz$, $\bar{\theta}_t = \int_0^t \theta_z dz$ for simplification when $s = 0$ and $\bar{\sigma}_{s:t}^2 = \lambda^2(1 - e^{-2\bar{\theta}_{s:t}})$, the forward process of GOUB is formed as:

$$d\mathbf{x}_t = \left(\theta_t + g_t^2 \frac{e^{-2\bar{\theta}_{t:T}}}{\bar{\sigma}_{t:T}^2} \right) (\mathbf{x}_T - \mathbf{x}_t) dt + g_t d\mathbf{w}_t. \quad (5)$$

And the forward transition $p(\mathbf{x}_t | \mathbf{x}_0, \mathbf{x}_T)$ is given by

$$p(\mathbf{x}_t | \mathbf{x}_0, \mathbf{x}_T) = \mathcal{N}(\bar{\boldsymbol{\mu}}'_t, \bar{\sigma}_t'^2 \mathbf{I}), \quad \bar{\boldsymbol{\mu}}'_t = e^{-\bar{\theta}_t} \frac{\bar{\sigma}_{t:T}^2}{\bar{\sigma}_T^2} \mathbf{x}_0 + (1 - e^{-\bar{\theta}_t} \frac{\bar{\sigma}_{t:T}^2}{\bar{\sigma}_T^2}) \mathbf{x}_T, \quad \bar{\sigma}_t'^2 = \frac{\bar{\sigma}_t^2 \bar{\sigma}_{t:T}^2}{\bar{\sigma}_T^2}. \quad (6)$$

Also, GOUB presents a new reverse ODE called Mean-ODE, which directly neglects the Brownian term of (3):

$$d\mathbf{x}_t = \left[\mathbf{f}(\mathbf{x}_t, t) + g_t^2 \nabla_{\mathbf{x}_t} \log p(\mathbf{x}_T | \mathbf{x}_t) - g_t^2 \nabla_{\mathbf{x}_t} \log p(\mathbf{x}_t | \mathbf{x}_T) \right] dt. \quad (7)$$

3.3 STOCHASTIC OPTIMAL CONTROL

Stochastic Optimal Control (SOC) is a mathematical discipline that focuses on determining optimal control strategies for dynamic systems under uncertainty. By integrating stochastic processes with optimization theory, SOC seeks to identify the best control strategies in scenarios involving randomness, as commonly encountered in fields like finance Geering et al. (2010) and style transfer Rout et al. (2024). Considering the dynamics described in (1), let us examine the following Linear Quadratic SOC problem Bryson (2018); O'Connell (2003); Kappen (2008); Chen et al. (2023):

$$\min_{\mathbf{u}_t, \gamma \in \mathcal{U}} \int_0^T \frac{1}{2} \|\mathbf{u}_{t,\gamma}\|_2^2 dt + \frac{\gamma}{2} \|\mathbf{x}_T^u - x_T\|_2^2 \quad \text{s.t.} \quad d\mathbf{x}_t = (\mathbf{f}(\mathbf{x}_t, t) + g_t \mathbf{u}_{t,\gamma}) dt + g_t d\mathbf{w}_t, \quad \mathbf{x}_0^u = x_0, \quad (8)$$

where \mathbf{x}_t^u is the diffusion process under control, x_0 and x_T represent for the initial state and the preset terminal respectively, $\|\mathbf{u}_{t,\gamma}\|_2^2$ is the instantaneous cost, $\frac{\gamma}{2} \|\mathbf{x}_T^u - x_T\|_2^2$ is the terminal cost with its penalty coefficient γ . The SOC problem aims to design the controller $\mathbf{u}_{t,\gamma}$ to drive the dynamic system from x_0 to x_T with minimum cost.

4 METHODS

4.1 DIFFUSION BRIDGES CONSTRUCTED BY SOC PROBLEM

The forward SDE of the Diffusion Bridge with Doob's h -transform is enforced to pass from the predetermined origin x_0 to the terminal x_T . With a similar purpose, UniDB constructs a SOC

problem where the constraints are an arbitrary linear SDE of the forward diffusion with a given initial state, while the objective incorporates a penalty term steering the forward diffusion trajectory towards the predetermined terminal x_T . Meanwhile, compared with the linear drift term (1), we combined a given state vector term \mathbf{m} with the same dimension as \mathbf{x}_t and its related coefficient h_t to improve the generality of the linear SDE form:

$$\mathbf{f}(\mathbf{x}_t, t) = f_t \mathbf{x}_t + h_t \mathbf{m}. \quad (9)$$

Accordingly, our SOC problem with unified linear SDE (9) is formed as:

$$\min_{\mathbf{u}_{t,\gamma} \in \mathcal{U}} \int_0^T \frac{1}{2} \|\mathbf{u}_{t,\gamma}\|_2^2 dt + \frac{\gamma}{2} \|\mathbf{x}_T^u - x_T\|_2^2 \quad \text{s.t.} \quad d\mathbf{x}_t = \left(f_t \mathbf{x}_t + h_t \mathbf{m} + g_t \mathbf{u}_{t,\gamma} \right) dt + g_t d\mathbf{w}_t, \quad \mathbf{x}_0^u = x_0. \quad (10)$$

According to the certainty equivalence principle Chen et al. (2023); Rout et al. (2024), the addition of noise or perturbations to a linear system with quadratic costs does not change the optimal control. Therefore, we can modify the SOC problem with the deterministic ODE condition to obtain the optimal controller $\mathbf{u}_{t,\gamma}^*$ as follows,

$$\min_{\mathbf{u}_{t,\gamma} \in \mathcal{U}} \int_0^T \frac{1}{2} \|\mathbf{u}_{t,\gamma}\|_2^2 dt + \frac{\gamma}{2} \|\mathbf{x}_T^u - x_T\|_2^2 \quad \text{s.t.} \quad d\mathbf{x}_t = \left(f_t \mathbf{x}_t + h_t \mathbf{m} + g_t \mathbf{u}_{t,\gamma} \right) dt, \quad \mathbf{x}_0^u = x_0. \quad (11)$$

We can derive the closed-form solution to the problem (11), which leads to the following Theorem 4.1:

Theorem 4.1. Consider the SOC problem (11), denote $d_{t,\gamma} = \gamma^{-1} + e^{2\bar{f}_t} \bar{g}_{t:T}^2$, $\bar{f}_{s:t} = \int_s^t f_z dz$, $\bar{h}_{s:t} = \int_s^t e^{-\bar{f}_z} h_z dz$ and $\bar{g}_{s:t}^2 = \int_s^t e^{-2\bar{f}_z} g_z^2 dz$, denote \bar{f}_t , \bar{h}_t and \bar{g}_t^2 for simplification when $s = 0$, then the closed-form optimal controller $\mathbf{u}_{t,\gamma}^*$ is

$$\mathbf{u}_{t,\gamma}^* = g_t e^{\bar{f}_{t:T}} \frac{x_T - e^{\bar{f}_{t:T}} \mathbf{x}_t - \mathbf{m} e^{\bar{f}_t} \bar{h}_{t:T}}{d_{t,\gamma}}, \quad (12)$$

and the transition of \mathbf{x}_t from x_0 and x_T is

$$\mathbf{x}_t = e^{\bar{f}_t} \left(\frac{d_{t,\gamma}}{d_{0,\gamma}} x_0 + \frac{e^{\bar{f}_t} \bar{g}_t^2}{d_{0,\gamma}} x_T + \left(\bar{h}_t - \frac{e^{2\bar{f}_t} \bar{h}_t \bar{g}_t^2}{d_{0,\gamma}} \right) \mathbf{m} \right). \quad (13)$$

The proof of Theorem 4.1 is provided in Appendix A.1. With Theorem 4.1, we can obtain an optimally controlled forward SDE connected from x_0 to the neighborhood of the terminal x_T and the transition of \mathbf{x}_t for the forward process. As for the backward process, similar to (3) and (7), the backward reverse SDE and Mean-ODE are respectively formulated as:

$$d\mathbf{x}_t = \left[f_t \mathbf{x}_t + h_t \mathbf{m} + g_t \mathbf{u}_{t,\gamma}^* - g_t^2 \nabla_{\mathbf{x}_t} \log p(\mathbf{x}_t | x_T) \right] dt + g_t d\tilde{\mathbf{w}}_t, \quad (14)$$

$$d\mathbf{x}_t = \left[f_t \mathbf{x}_t + h_t \mathbf{m} + g_t \mathbf{u}_{t,\gamma}^* - g_t^2 \nabla_{\mathbf{x}_t} \log p(\mathbf{x}_t | x_T) \right] dt. \quad (15)$$

4.2 CONNECTIONS BETWEEN SOC AND DOOB'S h -TRANSFORM

We can intuitively see from the SOC problem that when $\gamma \rightarrow \infty$ in Theorem 4.1, it means that the target of SDE process is precisely the predetermined endpoint Chen et al. (2023), which is also the purpose of Doob's h -transform and facilitates the following theorem:

Theorem 4.2. For the SOC problem (11), when $\gamma \rightarrow \infty$, the optimal controller becomes $\mathbf{u}_{t,\infty}^* = g_t \nabla_{\mathbf{x}_t} \log p(x_T | \mathbf{x}_t)$, and the corresponding forward and backward SDE with the linear SDE form (9) are the same as Doob's h -transform as in (2) and (3).

The proof of Theorem 4.2 is presented in Appendix A.2. This theorem shows that existing diffusion bridge models using Doob's h -transform are merely special instances of our UniDB framework, which offers a unified approach to diffusion bridges through the lens of SOC. Furthermore, using Doob's h -transform in diffusion bridge models is not necessarily optimal, as letting the terminal penalty coefficient $\gamma \rightarrow \infty$ eliminates the consideration of control costs in SOC.

4.3 TRAINING OBJECTIVE OF UNIDB

In this section, we focus on constructing the training objective of UniDB. According to maximum log-likelihood Ho et al. (2020) and conditional score matching Song et al. (2020), the training objective is based on the forward transition $p(\mathbf{x}_t | \mathbf{x}_0, \mathbf{x}_T)$. Thus, we begin by deriving this probability. The closed-form expression in (13) represents the mean value of the forward transition after applying reparameterization techniques. However, this expression lacks a noise component after the transformation based on the certainty equivalence principle. To address this issue, we employ stochastic interpolant theory Albergo et al. (2023) to introduce a noise term $\bar{\sigma}'_t \epsilon$ with $\bar{\sigma}'_0 = \bar{\sigma}'_T = 0$. We define $\bar{\sigma}'_t{}^2 = \bar{\sigma}_t^2 \bar{\sigma}_{t:T}^2 / \bar{\sigma}_T^2$ similar to (6) with $\bar{\sigma}_{s:t}^2 = e^{2\bar{f}_t} \bar{g}_{s:t}^2$, leading to the following forward transition:

$$p(\mathbf{x}_t | x_0, x_T) = \mathcal{N}(\bar{\boldsymbol{\mu}}_{t,\gamma}, \bar{\sigma}_t'^2 \mathbf{I}), \quad \bar{\boldsymbol{\mu}}_{t,\gamma} = e^{\bar{f}_t} \left(\frac{d_{t,\gamma}}{d_{0,\gamma}} x_0 + \frac{e^{\bar{f}_T} \bar{g}_t^2}{d_{0,\gamma}} x_T + \left(\bar{h}_t - \frac{e^{2\bar{f}_T} \bar{h}_T \bar{g}_t^2}{d_{0,\gamma}} \right) \mathbf{m} \right). \quad (16)$$

The detailed derivation is provided in Appendix A.3. Similar to Yue et al. (2023) using the l_1 loss form to bring improved visual quality and details at the pixel level Boyd (2004); Hastie et al. (2017), we can derive the training objective. Denote $a_{t,\gamma} = e^{\bar{f}_t} d_{t,\gamma}$, assuming $\boldsymbol{\mu}_{t-1,\theta}$, $\sigma_{t-1,\theta}^2$ and $\boldsymbol{\mu}_{t-1,\gamma}$, $\sigma_{t-1,\gamma}^2$ are respectively the mean values and variances of $p_\theta(\mathbf{x}_{t-1} | \mathbf{x}_t, x_T)$ and $p(\mathbf{x}_{t-1} | \mathbf{x}_0, \mathbf{x}_t, x_T)$, suppose the score $\nabla_{\mathbf{x}_t} \log p(\mathbf{x}_t | x_T)$ is parameterized as $-\epsilon_\theta(\mathbf{x}_t, x_T, t) / \bar{\sigma}'_t$, the final training objective is as follows,

$$\mathcal{L}_\theta = \mathbb{E}_{t, \mathbf{x}_0, \mathbf{x}_t, x_T} \left[\frac{1}{2\sigma_{t-1,\theta}^2} \left\| \boldsymbol{\mu}_{t-1,\theta} - \boldsymbol{\mu}_{t-1,\gamma} \right\|_1 \right], \quad \sigma_{t-1,\theta} = g_t,$$

$$\boldsymbol{\mu}_{t-1,\theta} = \mathbf{x}_t - f_t \mathbf{x}_t - h_t \mathbf{m} - g_t \mathbf{u}_{t,\gamma}^* + \frac{g_t^2}{\bar{\sigma}'_t} \epsilon_\theta(\mathbf{x}_t, x_T, t), \quad \boldsymbol{\mu}_{t-1,\gamma} = \bar{\boldsymbol{\mu}}_{t-1,\gamma} + \frac{\bar{\sigma}_{t-1}^2 a_{t,\gamma}}{\bar{\sigma}'_t^2 a_{t-1,\gamma}} (\mathbf{x}_t - \bar{\boldsymbol{\mu}}_{t,\gamma}). \quad (17)$$

Please refer to Appendix A.4 for detailed derivations. Therefore, we can recover or generate the origin image \hat{x}_0 through Euler sampling iterations. So far, we've built the UniDB framework, which establishes and expands the forward and backward process of the diffusion bridge model through SOC and comprises Doob's h -transform as a special case.

4.4 UNIDB UNIFIES DIFFUSION BRIDGE MODELS

Our UniDB is a unified framework for existing diffusion bridge models: DDBMs (VE) Zhou et al. (2023), DDBMs (VP) Zhou et al. (2023) and GOUB Yue et al. (2023).

Proposition 4.3. *UniDB encompasses existing diffusion bridge models by employing different hyperparameter spaces \mathcal{H} as follows:*

- DDBMs (VE) corresponds to UniDB with hyperparameter $\mathcal{H}_{VE}(f_t = 0, h_t = 0, \gamma \rightarrow \infty)$
- DDBMs (VP) corresponds to UniDB with hyperparameter $\mathcal{H}_{VP}(f_t = -\frac{g_t^2}{2}, h_t = 0, \gamma \rightarrow \infty)$
- GOUB corresponds to UniDB with hyperparameter $\mathcal{H}_{GOU}(f_t = -h_t = \theta_t, \mathbf{m} = \boldsymbol{\mu}, \gamma \rightarrow \infty)$

4.5 AN EXAMPLE: UNIDB-GOU

It is evident that these diffusion bridge models like DDBMs (VE), DDBMs (VP) and GOUB all based on Doob's h -transform are all special cases of UniDB with $\gamma \rightarrow \infty$. We introduce UniDB based on the GOU process (4) as an example, hereafter referred to as UniDB-GOU, which retains the penalty coefficient γ as the hyper-parameter. Considering the SOC problem with GOU process (4), the optimally controlled forward SDE and the mean value of forward transition $p(\mathbf{x}_t | x_0, x_T)$ are respectively:

$$d\mathbf{x}_t = \left(\theta_t + \frac{g_t^2 e^{-2\bar{\theta}_t T}}{\gamma^{-1} + \bar{\sigma}_{t:T}^2} \right) (x_T - \mathbf{x}_t) dt + g_t d\mathbf{w}_t, \quad \bar{\boldsymbol{\mu}}_{t,\gamma} = e^{-\bar{\theta}_t} \frac{1 + \gamma \bar{\sigma}_{t:T}^2}{1 + \gamma \bar{\sigma}_T^2} x_0 + (1 - e^{-\bar{\theta}_t} \frac{1 + \gamma \bar{\sigma}_{t:T}^2}{1 + \gamma \bar{\sigma}_T^2}) x_T. \quad (18)$$

Please refer to Appendix A.5 for detailed proof. It's worth noting that our UniDB model can be a plugin module to the existing diffusion bridge with Doob's h -transform. Taking UniDB-GOU as an

example, we highlight the key difference between UniDB-GOU and GOUB (the coefficient of x_0 in the mean value of forward transition and h -function term) as follows:

$$\underbrace{e^{-\bar{\theta}_t} \frac{\bar{\sigma}_{t:T}^2}{\bar{\sigma}_T^2}, g_t \mathbf{h} = \frac{g_t e^{-2\bar{\theta}_{t:T}} (x_T - \mathbf{x}_t)}{\bar{\sigma}_{t:T}^2}}_{\text{GOUB}} \Rightarrow \underbrace{e^{-\bar{\theta}_t} \frac{\gamma^{-1} + \bar{\sigma}_{t:T}^2}{\gamma^{-1} + \bar{\sigma}_T^2}, \mathbf{u}_{t,\gamma}^* = \frac{g_t e^{-2\bar{\theta}_{t:T}} (x_T - \mathbf{x}_t)}{\gamma^{-1} + \bar{\sigma}_{t:T}^2}}_{\text{UniDB-GOU}}. \quad (19)$$

Hence, only a few lines of code need to be adjusted to generate more realistic images using the same training method. We provide a pseudo-code for the training process of UniDB-GOU as follows.

Algorithm 1 UniDB Training

repeat

Take a pair of images $\mathbf{x}_0 = x_0, \mathbf{x}_T = x_T$

$t \sim \text{Uniform}(\{1, \dots, T\})$

$\sigma_{t-1,\theta} = g_t$

$a_{t,\gamma} = e^{-\bar{\theta}_t} \frac{\bar{\sigma}_{t:T}^2}{\bar{\sigma}_T^2} \leftarrow \text{GOUB}$

$a_{t,\gamma} = e^{-\bar{\theta}_t} \frac{\gamma^{-1} + \bar{\sigma}_{t:T}^2}{\gamma^{-1} + \bar{\sigma}_T^2} \leftarrow \text{UniDB-GOU}$

$\mathbf{x}_t = a_{t,\gamma} x_0 + (1 - a_{t,\gamma}) x_T + \bar{\sigma}'_t \epsilon$

$\bar{\boldsymbol{\mu}}_{t,\gamma} = a_{t,\gamma} x_0 + (1 - a_{t,\gamma}) x_T$

$\boldsymbol{\mu}_{t-1,\theta} = \mathbf{x}_t - \left(\theta_t + g_t^2 \frac{e^{-2\bar{\theta}_{t:T}}}{\bar{\sigma}_{t:T}^2} \right) (x_T - \mathbf{x}_t) + \frac{g_t^2}{\bar{\sigma}_t^2} \epsilon_\theta(\mathbf{x}_t, x_T, t) \leftarrow \text{GOUB}$

$\boldsymbol{\mu}_{t-1,\theta} = \mathbf{x}_t - \left(\theta_t + g_t^2 \frac{e^{-2\bar{\theta}_{t:T}}}{\gamma^{-1} + \bar{\sigma}_{t:T}^2} \right) (x_T - \mathbf{x}_t) + \frac{g_t^2}{\bar{\sigma}_t^2} \epsilon_\theta(\mathbf{x}_t, x_T, t) \leftarrow \text{UniDB + GOU}$

$\boldsymbol{\mu}_{t-1,\gamma} = \bar{\boldsymbol{\mu}}_{t-1,\gamma} + \frac{\bar{\sigma}'_{t-1} a_{t,\gamma}}{\bar{\sigma}_t^2 a_{t-1,\gamma}} (\mathbf{x}_t - \bar{\boldsymbol{\mu}}_{t,\gamma})$

Take gradient descent step on $\nabla_\theta \left(\mathcal{L}_\theta = \mathbb{E}_{t,\mathbf{x}_0,\mathbf{x}_t,\mathbf{x}_T} \left[\frac{1}{2\sigma_{t-1,\theta}^2} \|\boldsymbol{\mu}_{t-1,\theta} - \boldsymbol{\mu}_{t-1,\gamma}\|^2 \right] \right)$

until converged

5 EXPERIMENTS

In this section, we evaluate our models in image restoration tasks including Image 4× Super-resolution, Image Deraining, and Image Inpainting. For simple expressions in the following sections, UniDB (SDE) and UniDB (ODE) are applied to represent the UniDB-GOU with reverse SDE and reverse Mean-ODE, respectively. Please refer to Appendix B and C for all related implementation details and more experiment results, respectively.

Table 1: Qualitative comparison with the relevant baselines on DIV2K, Rain100H, and CelebA-HQ.

METHOD	Image Super-Resolution				METHOD	Image Deraining				METHOD	Image Inpainting			
	PSNR↑	SSIM↑	LPIPS↓	FID↓		PSNR↑	SSIM↑	LPIPS↓	FID↓		PSNR↑	SSIM↑	LPIPS↓	FID↓
Bicubic	26.70	0.774	0.425	36.18	MAXIM	30.81	0.902	0.133	58.72	PromptIR	30.22	0.918	0.068	32.69
DDRM	24.35	0.592	0.364	78.71	MHNet	31.08	0.899	0.126	57.93	DDRM	27.16	0.899	0.089	37.02
IR-SDE	25.90	0.657	0.231	45.36	IR-SDE	31.65	0.904	0.047	18.64	IR-SDE	28.37	0.916	0.046	25.13
GOUB (SDE)	26.89	0.7478	0.220	20.85	GOUB (SDE)	31.96	0.9028	0.046	18.14	GOUB (SDE)	28.98	0.9067	0.037	4.30
GOUB (ODE)	28.50	0.8070	0.328	22.14	GOUB (ODE)	34.56	0.9414	0.077	32.83	GOUB (ODE)	31.39	0.9392	0.052	12.24
UniDB (SDE)	25.46	0.6856	0.179	16.21	UniDB (SDE)	32.05	0.9036	0.045	17.65	UniDB (SDE)	29.20	0.9077	0.036	4.08
UniDB (ODE)	28.64	0.8072	0.323	22.32	UniDB (ODE)	34.68	0.9426	0.074	31.16	UniDB (ODE)	31.67	0.9395	0.052	11.98

Image 4× Super-Resolution Tasks. In super-resolution, we evaluated our models based on DIV2K dataset Agustsson & Timofte (2017), which contains 2K-resolution high-quality images. During the experiment, all low-resolution images were 4× bicubic upscaling to the same image size as the paired high-resolution images. For comparison, we choose Bicubic interpolation Kawar et al. (2022), DDRM Kawar et al. (2022), IR-SDE Luo et al. (2023), GOUB (SDE) Yue et al. (2023) and GOUB (Mean-ODE) Yue et al. (2023) following abbreviated as GOUB (ODE) as the baselines. The qualitative and quantitative results are illustrated in Table 1 and Figure 2 in Appendix C. Visually, our proposed model demonstrates a significant improvement over the baseline across various metrics. It also excels by delivering superior performance in both visual quality and detail compared to other results.

Image Deraining Tasks. For image deraining tasks, we conducted the experiments based on Rain100H datasets Yang et al. (2017). Particularly, to be consistent with other deraining models Ren et al. (2019); Zamir et al. (2021); Luo et al. (2023); Yue et al. (2023), PSNR and SSIM scores on the Y channel (YCbCr space) are selected instead of the origin PSNR and SSIM. MAXIM Tu et al. (2022), MHNet Gao et al. (2025), IR-SDE Luo et al. (2023), GOUB (SDE) Yue et al. (2023) and GOUB (ODE) Yue et al. (2023) are chosen as the baselines. The relevant experimental results are shown in the Table 1 and Figure 2 in Appendix C. Similarly, our model achieved state-of-the-art results in the deraining task. Visually, it can also be observed that our model excels in capturing details such as the eyebrows, eye bags, and lips.

Image Inpainting Tasks. In image inpainting tasks, we evaluated our methods on CelebA-HQ 256×256 datasets Karras (2017). For comparison, we choose DDRM Kawar et al. (2022), PromptIR Potlapalli et al. (2023), IR-SDE Luo et al. (2023), GOUB (SDE) Yue et al. (2023) and GOUB (ODE) Yue et al. (2023) as the baselines. As for mask type, we take 100 thin masks consistent with the baselines. The relevant experimental results are shown in Table 1 and Figure 2 in Appendix C. It is observed that our model achieved state-of-the-art results in all indicators and also delivered highly competitive outcomes on other metrics. From a visual perspective, our model excels in capturing details such as faces, eyes, chins, and noses.

5.1 ABLATION STUDY

Penalty Coefficient γ . To evaluate the specific impact of different penalty coefficients γ on model performance, we conducted the experiments with several different γ . The final results are shown in Table 2. The results across all tasks show that the choice of γ significantly influences the model’s performance on all tasks, different optimal γ for different tasks, and our UniDB achieves the best performance in almost all metrics. Particularly in super-resolution tasks, we focus on the significantly better perceptual scores (LPIPS and FID) Luo et al. (2023), demonstrating that UniDB ensures to capture and preserve more intricate image details and features as shown in Figure 2. These findings underscore the importance of carefully tuning γ to achieve the best performance for specific tasks.

Table 2: Qualitative comparison with the different bridge models on CelebA-HQ, Rain100H, and DIV2K datasets.

Different γ	Image 4×Super-Resolution				Image Deraining				Image Inpainting			
	PSNR \uparrow	SSIM \uparrow	LPIPS \downarrow	FID \downarrow	PSNR \uparrow	SSIM \uparrow	LPIPS \downarrow	FID \downarrow	PSNR \uparrow	SSIM \uparrow	LPIPS \downarrow	FID \downarrow
5×10^5	24.94	0.6419	0.234	20.33	28.73	0.9065	0.038	4.49	29.44	0.8715	0.058	24.96
1×10^6	24.72	0.6587	0.199	18.37	29.15	0.9068	0.036	4.12	31.96	0.9018	0.045	18.37
1×10^7	25.46	0.6856	0.179	16.21	29.20	0.9077	0.036	4.08	32.00	0.9029	0.046	17.87
1×10^8	25.06	0.6393	0.289	23.76	28.65	0.9062	0.039	4.64	32.05	0.9036	0.045	17.65
∞	26.89	0.7478	0.220	20.85	28.98	0.9067	0.037	4.30	31.96	0.9028	0.046	18.14

6 CONCLUSION

In this paper, we presented UniDB, a unified diffusion bridge framework based on stochastic optimal control principles, offering a novel perspective on diffusion bridges. Through this framework, we unify and extend existing diffusion bridge models with Doob’s h -transform like DDBMs and GOUB. Moreover, we demonstrate that the diffusion bridge with Doob’s h -transform can be viewed as a specific case within UniDB when the terminal penalty coefficient approaches infinity. This insight helps elucidate why Doob’s h -transform may lead to suboptimal image restoration, often resulting in blurred or distorted details. By simply adjusting this terminal penalty coefficient, UniDB achieves a marked improvement in image quality with minimal code modifications. Our experimental results underscore UniDB’s superiority and versatility across various image processing tasks, particularly in enhancing image details for more realistic outputs. Despite these advantages, UniDB, like other standard diffusion bridge models, faces the challenge of computationally intensive sampling processes, especially with high-resolution images or complex restoration tasks. Future work will focus on developing strategies to accelerate the sampling process, enhancing UniDB’s practicality, particularly for real-time applications.

ACKNOWLEDGEMENT

This work was supported by the National Natural Science Foundation of China (No.62303319, No.62406195), Shanghai Local College Capacity Building Program (23010503100), ShanghaiTech AI4S Initiative SHTAI4S202404, HPC Platform of ShanghaiTech University, MoE Key Laboratory of Intelligent Perception and Human-Machine Collaboration (ShanghaiTech University) and Shanghai Engineering Research Center of Intelligent Vision and Imaging.

REFERENCES

- Eirikur Agustsson and Radu Timofte. Ntire 2017 challenge on single image super-resolution: Dataset and study. In *Proceedings of the IEEE conference on computer vision and pattern recognition workshops*, pp. 126–135, 2017.
- R Ahmad. Introduction to stochastic differential equations, 1988.
- Michael S Albergo, Nicholas M Boffi, and Eric Vanden-Eijnden. Stochastic interpolants: A unifying framework for flows and diffusions. *arXiv preprint arXiv:2303.08797*, 2023.
- Brian DO Anderson. Reverse-time diffusion equation models. *Stochastic Processes and their Applications*, 12(3):313–326, 1982.
- Julius Berner, Lorenz Richter, and Karen Ullrich. An optimal control perspective on diffusion-based generative modeling. *arXiv preprint arXiv:2211.01364*, 2022.
- Stephen Boyd. Convex optimization. *Cambridge UP*, 2004.
- Arwen Bradley and Preetum Nakkiran. Classifier-free guidance is a predictor-corrector. *arXiv preprint arXiv:2408.09000*, 2024.
- Arthur Earl Bryson. *Applied optimal control: optimization, estimation and control*. Routledge, 2018.
- Tianrong Chen, Jiatao Gu, Laurent Dinh, Evangelos A Theodorou, Joshua Susskind, and Shuangfei Zhai. Generative modeling with phase stochastic bridges. *arXiv preprint arXiv:2310.07805*, 2023.
- Cheng Chi, Zhenjia Xu, Siyuan Feng, Eric Cousineau, Yilun Du, Benjamin Burchfiel, Russ Tedrake, and Shuran Song. Diffusion policy: Visuomotor policy learning via action diffusion. *The International Journal of Robotics Research*, pp. 02783649241273668, 2023.
- Hyungjin Chung, Jeongsol Kim, Michael T Mccann, Marc L Klasky, and Jong Chul Ye. Diffusion posterior sampling for general noisy inverse problems. *arXiv preprint arXiv:2209.14687*, 2022.
- Valentin De Bortoli, James Thornton, Jeremy Heng, and Arnaud Doucet. Diffusion schrödinger bridge with applications to score-based generative modeling. *Advances in Neural Information Processing Systems*, 34:17695–17709, 2021.
- Prafulla Dhariwal and Alexander Nichol. Diffusion models beat gans on image synthesis. *Advances in neural information processing systems*, 34:8780–8794, 2021.
- Shutong Ding, Ke Hu, Zhenhao Zhang, Kan Ren, Weinan Zhang, Jingyi Yu, Jingya Wang, and Ye Shi. Diffusion-based reinforcement learning via q-weighted variational policy optimization. In *The Thirty-eighth Annual Conference on Neural Information Processing Systems*, 2024a.
- Xin Ding, Yongwei Wang, Kao Zhang, and Z Jane Wang. Ccdm: Continuous conditional diffusion models for image generation. *arXiv preprint arXiv:2405.03546*, 2024b.
- Hu Gao, Ying Zhang, Jing Yang, and Depeng Dang. Mixed hierarchy network for image restoration. *Pattern Recognition*, 161:111313, 2025.
- Hans P Geering, Florian Herzog, and Gabriel Dondi. Stochastic optimal control with applications in financial engineering. *Optimization and Optimal Control: Theory and Applications*, pp. 375–408, 2010.

- Trevor Hastie, Robert Tibshirani, and Jerome Friedman. The elements of statistical learning: data mining, inference, and prediction, 2017.
- Jonathan Ho and Tim Salimans. Classifier-free diffusion guidance. *arXiv preprint arXiv:2207.12598*, 2022.
- Jonathan Ho, Ajay Jain, and Pieter Abbeel. Denoising diffusion probabilistic models. *Advances in neural information processing systems*, 33:6840–6851, 2020.
- HJ Kappen. Stochastic optimal control theory. *ICML, Helsinki, Radboud University, Nijmegen, Netherlands*, 2008.
- Tero Karras. Progressive growing of gans for improved quality, stability, and variation. *arXiv preprint arXiv:1710.10196*, 2017.
- Bahjat Kawar, Michael Elad, Stefano Ermon, and Jiaming Song. Denoising diffusion restoration models. *Advances in Neural Information Processing Systems*, 35:23593–23606, 2022.
- Diederik P Kingma. Adam: A method for stochastic optimization. *arXiv preprint arXiv:1412.6980*, 2014.
- Donald E Kirk. *Optimal control theory: an introduction*. Courier Corporation, 2004.
- W. Levine. Optimal control theory: An introduction. *IEEE Transactions on Automatic Control*, 17(3):423–423, 1972. doi: 10.1109/TAC.1972.1100008.
- Xin Li, Yulin Ren, Xin Jin, Cuiling Lan, Xingrui Wang, Wenjun Zeng, Xinchao Wang, and Zhibo Chen. Diffusion models for image restoration and enhancement—a comprehensive survey. *arXiv preprint arXiv:2308.09388*, 2023.
- Ziwei Luo, Fredrik K Gustafsson, Zheng Zhao, Jens Sjölund, and Thomas B Schön. Image restoration with mean-reverting stochastic differential equations. *arXiv preprint arXiv:2301.11699*, 2023.
- Naoki Murata, Koichi Saito, Chieh-Hsin Lai, Yuhta Takida, Toshimitsu Uesaka, Yuki Mitsufuji, and Stefano Ermon. Gibbsddrm: A partially collapsed gibbs sampler for solving blind inverse problems with denoising diffusion restoration. In *International conference on machine learning*, pp. 25501–25522. PMLR, 2023.
- Alexander Quinn Nichol and Prafulla Dhariwal. Improved denoising diffusion probabilistic models. In *International conference on machine learning*, pp. 8162–8171. PMLR, 2021.
- Neil O’Connell. Conditioned random walks and the rsk correspondence. *Journal of Physics A: Mathematical and General*, 36(12):3049, 2003.
- Byoungwoo Park, Jungwon Choi, Sungbin Lim, and Juho Lee. Stochastic optimal control for diffusion bridges in function spaces. *arXiv preprint arXiv:2405.20630*, 2024.
- Vaishnav Potlapalli, Syed Waqas Zamir, Salman Khan, and Fahad Shahbaz Khan. Promptir: Prompting for all-in-one blind image restoration. *arXiv preprint arXiv:2306.13090*, 2023.
- Dongwei Ren, Wangmeng Zuo, Qinghua Hu, Pengfei Zhu, and Deyu Meng. Progressive image deraining networks: A better and simpler baseline. In *Proceedings of the IEEE/CVF conference on computer vision and pattern recognition*, pp. 3937–3946, 2019.
- Litu Rout, Yujia Chen, Nataniel Ruiz, Abhishek Kumar, Constantine Caramanis, Sanjay Shakkottai, and Wen-Sheng Chu. Rb-modulation: Training-free personalization of diffusion models using stochastic optimal control. *arXiv preprint arXiv:2405.17401*, 2024.
- Simo Särkkä and Arno Solin. *Applied stochastic differential equations*, volume 10. Cambridge University Press, 2019.
- Rahul Shenoy, Zhihong Pan, Kaushik Balakrishnan, Qisen Cheng, Yongmoon Jeon, Heejune Yang, and Jaewon Kim. Gradient-free classifier guidance for diffusion model sampling. *arXiv preprint arXiv:2411.15393*, 2024.

- Yuyang Shi, Valentin De Bortoli, Andrew Campbell, and Arnaud Doucet. Diffusion schrödinger bridge matching. *Advances in Neural Information Processing Systems*, 36, 2024.
- Jascha Sohl-Dickstein, Eric Weiss, Niru Maheswaranathan, and Surya Ganguli. Deep unsupervised learning using nonequilibrium thermodynamics. In *International conference on machine learning*, pp. 2256–2265. PMLR, 2015.
- Vignesh Ram Somnath, Matteo Pariset, Ya-Ping Hsieh, Maria Rodriguez Martinez, Andreas Krause, and Charlotte Bunne. Aligned diffusion schrödinger bridges. In *Uncertainty in Artificial Intelligence*, pp. 1985–1995. PMLR, 2023.
- Yang Song and Stefano Ermon. Generative modeling by estimating gradients of the data distribution. *Advances in neural information processing systems*, 32, 2019.
- Yang Song, Jascha Sohl-Dickstein, Diederik P Kingma, Abhishek Kumar, Stefano Ermon, and Ben Poole. Score-based generative modeling through stochastic differential equations. *arXiv preprint arXiv:2011.13456*, 2020.
- Jiangnan Tang, Jingya Wang, Kaiyang Ji, Lan Xu, Jingyi Yu, and Ye Shi. A unified diffusion framework for scene-aware human motion estimation from sparse signals. In *Proceedings of the IEEE/CVF Conference on Computer Vision and Pattern Recognition*, pp. 21251–21262, 2024.
- Zhengzhong Tu, Hossein Talebi, Han Zhang, Feng Yang, Peyman Milanfar, Alan Bovik, and Yinxiao Li. Maxim: Multi-axis mlp for image processing. In *Proceedings of the IEEE/CVF conference on computer vision and pattern recognition*, pp. 5769–5780, 2022.
- Shijie Wu, Yihang Zhu, Yunao Huang, Kaizhen Zhu, Jiayuan Gu, Jingyi Yu, Ye Shi, and Jingya Wang. Afforddp: Generalizable diffusion policy with transferable affordance. *arXiv preprint arXiv:2412.03142*, 2024.
- Bin Xia, Yulun Zhang, Shiyin Wang, Yitong Wang, Xinglong Wu, Yapeng Tian, Wenming Yang, and Luc Van Gool. Diffir: Efficient diffusion model for image restoration. In *Proceedings of the IEEE/CVF International Conference on Computer Vision*, pp. 13095–13105, 2023.
- Lingxiao Yang, Shutong Ding, Yifan Cai, Jingyi Yu, Jingya Wang, and Ye Shi. Guidance with spherical gaussian constraint for conditional diffusion. In *International Conference on Machine Learning*, 2024.
- Long Yang, Zhixiong Huang, Fenghao Lei, Yucun Zhong, Yiming Yang, Cong Fang, Shiting Wen, Binbin Zhou, and Zhouchen Lin. Policy representation via diffusion probability model for reinforcement learning. *arXiv preprint arXiv:2305.13122*, 2023.
- Wenhan Yang, Robby T Tan, Jiashi Feng, Jiaying Liu, Zongming Guo, and Shuicheng Yan. Deep joint rain detection and removal from a single image. In *Proceedings of the IEEE conference on computer vision and pattern recognition*, pp. 1357–1366, 2017.
- Conghan Yue, Zhengwei Peng, Junlong Ma, Shiyan Du, Pengxu Wei, and Dongyu Zhang. Image restoration through generalized ornstein-uhlenbeck bridge. *arXiv preprint arXiv:2312.10299*, 2023.
- Syed Waqas Zamir, Aditya Arora, Salman Khan, Munawar Hayat, Fahad Shahbaz Khan, Ming-Hsuan Yang, and Ling Shao. Multi-stage progressive image restoration. In *Proceedings of the IEEE/CVF conference on computer vision and pattern recognition*, pp. 14821–14831, 2021.
- Yanjie Ze, Gu Zhang, Kangning Zhang, Chenyuan Hu, Muhan Wang, and Huazhe Xu. 3d diffusion policy: Generalizable visuomotor policy learning via simple 3d representations. In *ICRA 2024 Workshop on 3D Visual Representations for Robot Manipulation*, 2024.
- Kaiwen Zheng, Guande He, Jianfei Chen, Fan Bao, and Jun Zhu. Diffusion bridge implicit models. *arXiv preprint arXiv:2405.15885*, 2024.
- Linqi Zhou, Aaron Lou, Samar Khanna, and Stefano Ermon. Denoising diffusion bridge models. *arXiv preprint arXiv:2309.16948*, 2023.

APPENDIX CONTENTS

- Appendix A: Proof Page 12
 - A.1 Proof of Theorem 4.1 Page 12
 - A.2 Proof of Theorem 4.2 Page 13
 - A.3 Derivation of the transition probability (16) Page 14
 - A.4 Derivation of the training objective (17) Page 15
 - A.5 Derivation of UniDB-GOU Page 17
- Appendix B: Implementation Details Page 18
- Appendix C: Additional Experimental Results Page 19

A PROOF

A.1 PROOF OF THEOREM 4.1

Theorem 4.1. Consider the SOC problem (11), denote $d_{t,\gamma} = \gamma^{-1} + e^{2\bar{f}_T} \bar{g}_{t:T}^2$, $\bar{f}_{s:t} = \int_s^t f_z dz$, $\bar{h}_{s:t} = \int_s^t e^{-\bar{f}_z} h_z dz$ and $\bar{g}_{s:t}^2 = \int_s^t e^{-2\bar{f}_z} g_z^2 dz$, denote \bar{f}_t , \bar{h}_t and \bar{g}_t^2 for simplification when $s = 0$, then the closed-form optimal controller $\mathbf{u}_{t,\gamma}^*$ is

$$\mathbf{u}_{t,\gamma}^* = g_t e^{\bar{f}_{t:T}} \frac{x_T - e^{\bar{f}_{t:T}} \mathbf{x}_t - \mathbf{m} e^{\bar{f}_T} \bar{h}_{t:T}}{d_{t,\gamma}}, \quad (12)$$

and the transition of \mathbf{x}_t from x_0 and x_T is

$$\mathbf{x}_t = e^{\bar{f}_t} \left(\frac{d_{t,\gamma}}{d_{0,\gamma}} x_0 + \frac{e^{\bar{f}_T} \bar{g}_t^2}{d_{0,\gamma}} x_T + \left(\bar{h}_t - \frac{e^{2\bar{f}_T} \bar{h}_T \bar{g}_t^2}{d_{0,\gamma}} \right) \mathbf{m} \right). \quad (13)$$

Proof. According to Pontryagin Maximum Principle Levine (1972); Kirk (2004) recipe, one can construct the Hamiltonian:

$$H(t, \mathbf{x}_t, \mathbf{u}_{t,\gamma}, \mathbf{p}_t) = \frac{1}{2} \|\mathbf{u}_{t,\gamma}\|_2^2 + \mathbf{p}_t^T (f_t \mathbf{x}_t + h_t \mathbf{m} + g_t \mathbf{u}_t). \quad (20)$$

By setting:

$$\frac{\partial H}{\partial \mathbf{u}_{t,\gamma}} = 0 \quad \Rightarrow \quad \mathbf{u}_{t,\gamma}^* = -g_t \mathbf{p}_t. \quad (21)$$

Then the value function becomes

$$V^* = \min_{\mathbf{u}_{t,\gamma}} H(t, \mathbf{x}_t, \mathbf{p}_t, \mathbf{u}_{t,\gamma}) = H(t, \mathbf{x}_t, \mathbf{p}_t, \mathbf{u}_{t,\gamma}^*) = -\frac{g_t^2}{2} \|\mathbf{p}_t\|_2^2 + f_t \mathbf{p}_t^T \mathbf{x}_t + h_t \mathbf{p}_t^T \mathbf{m}. \quad (22)$$

Now, according to minimum principle theorem to obtain the following set of differential equations:

$$\frac{d\mathbf{x}_t}{dt} = \nabla_{\mathbf{p}_t} H(\mathbf{x}_t, \mathbf{p}_t, \mathbf{u}_{t,\gamma}^*, t) = -g_t^2 \mathbf{p}_t + f_t \mathbf{x}_t + h_t \mathbf{m}, \quad (23)$$

$$\frac{d\mathbf{p}_t}{dt} = -\nabla_{\mathbf{x}_t} H(\mathbf{x}_t, \mathbf{p}_t, \mathbf{u}_{t,\gamma}^*, t) = -\mathbf{p}_t f_t, \quad (24)$$

$$\mathbf{x}_0 = x_0, \quad (25)$$

$$\mathbf{p}_T = \gamma (\mathbf{x}_T - x_T). \quad (26)$$

Solving the Equation (24), we have:

$$\begin{aligned} \mathbf{p}_t &= \mathbf{p}_0 e^{-\bar{f}_t}, \\ \mathbf{p}_T &= \mathbf{p}_0 e^{-\bar{f}_T}. \end{aligned} \quad (27)$$

Solve the Equation (23):

$$\begin{aligned}
\frac{d\mathbf{x}_t}{dt} &= f_t\mathbf{x}_t + h_t\mathbf{m} - g_t^2\mathbf{p}_t \\
\Rightarrow \frac{d(e^{-\bar{f}_t}\mathbf{x}_t)}{dt} &= e^{-\bar{f}_t}h_t\mathbf{m} - e^{-\bar{f}_t}g_t^2\mathbf{p}_t, \\
\Rightarrow e^{-\bar{f}_t}\mathbf{x}_t - \mathbf{x}_0 &= \mathbf{m}\bar{h}_t - \mathbf{p}_0\bar{g}_t^2, \\
\Rightarrow e^{-\bar{f}_t}\mathbf{x}_t - x_0 &= \mathbf{m}\bar{h}_t - \mathbf{p}_0\bar{g}_t^2.
\end{aligned}$$

Hence, we can get:

$$\mathbf{x}_T = e^{\bar{f}_T}x_0 + \mathbf{m}e^{\bar{f}_T}\bar{h}_T - \mathbf{p}_T e^{2\bar{f}_T}\bar{g}_T^2, \quad (28)$$

and

$$\mathbf{x}_t = e^{\bar{f}_t}x_0 + \mathbf{m}e^{\bar{f}_t}\bar{h}_t - \mathbf{p}_T e^{\bar{f}_t}e^{\bar{f}_T}\bar{g}_t^2. \quad (29)$$

Take the Equation (28) into the Equation (26) and solve \mathbf{p}_T ,

$$\mathbf{p}_T = \gamma \left(e^{\bar{f}_T}x_0 + \mathbf{m}e^{\bar{f}_T}\bar{h}_T - \mathbf{p}_T e^{2\bar{f}_T}\bar{g}_T^2 - x_T \right) \quad (30)$$

$$\Rightarrow \mathbf{p}_T = \frac{\gamma \left(e^{\bar{f}_T}x_0 + \mathbf{m}e^{\bar{f}_T}\bar{h}_T - x_T \right)}{1 + \gamma e^{2\bar{f}_T}\bar{g}_T^2}. \quad (31)$$

Also, take the Equation (30) into the equation (29),

$$\begin{aligned}
\mathbf{x}_t &= e^{\bar{f}_t}x_0 + \mathbf{m}e^{\bar{f}_t}\bar{h}_t - e^{\bar{f}_t}e^{\bar{f}_T}\bar{g}_t^2 \frac{e^{\bar{f}_T}x_0 + \mathbf{m}e^{\bar{f}_T}\bar{h}_T - x_T}{\gamma^{-1} + e^{2\bar{f}_T}\bar{g}_T^2}, \\
&= e^{\bar{f}_t} \left(\frac{d_{t,\gamma}}{d_{0,\gamma}}x_0 + \frac{e^{\bar{f}_T}\bar{g}_t^2}{d_{0,\gamma}}x_T + \left(\bar{h}_t - \frac{e^{2\bar{f}_T}\bar{h}_T\bar{g}_t^2}{d_{0,\gamma}} \right) \mathbf{m} \right).
\end{aligned} \quad (32)$$

Preserve γ ,

$$\begin{aligned}
\mathbf{u}_{t,\gamma}^* &= -g_t\mathbf{p}_t, \\
&= -g_t e^{-\bar{f}_t} e^{\bar{f}_T} \frac{e^{\bar{f}_T}x_0 + \mathbf{m}e^{\bar{f}_T}\bar{h}_T - x_T}{\gamma^{-1} + e^{2\bar{f}_T}\bar{g}_T^2}, \\
&= -g_t e^{-\bar{f}_t} e^{\bar{f}_T} \frac{e^{\bar{f}_T}x_0 + \mathbf{m}e^{\bar{f}_T}\bar{h}_T - x_T}{\gamma^{-1} + e^{2\bar{f}_T}\bar{g}_T^2}, \\
&= g_t e^{\bar{f}_{t:T}} \frac{x_T - e^{\bar{f}_{t:T}}\mathbf{x}_t - \mathbf{m}e^{\bar{f}_T}\bar{h}_{t:T}}{d_{t,\gamma}},
\end{aligned} \quad (33)$$

with the fact (32)

$$\mathbf{x}_t = e^{\bar{f}_t} \left(\frac{d_{t,\gamma}}{d_{0,\gamma}}x_0 + \frac{e^{\bar{f}_T}\bar{g}_t^2}{d_{0,\gamma}}x_T + \left(\bar{h}_t - \frac{e^{2\bar{f}_T}\bar{h}_T\bar{g}_t^2}{d_{0,\gamma}} \right) \mathbf{m} \right), \quad (34)$$

which concludes the proof of the Proposition 4.1. \square

A.2 PROOF OF THEOREM 4.2

Theorem 4.2. *For the SOC problem (11), when $\gamma \rightarrow \infty$, the optimal controller becomes $\mathbf{u}_{t,\infty}^* = g_t \nabla_{\mathbf{x}_t} \log p(\mathbf{x}_T | \mathbf{x}_t)$, and the corresponding forward and backward SDE with the linear SDE form (9) are the same as Doob's h-transform as in (2) and (3).*

Proof. Since in Proposition 4.1 we have solved the control problem and the optimal controller $\mathbf{u}_{t,\infty}^*$ is:

$$\mathbf{u}_{t,\infty}^* = \lim_{\gamma \rightarrow \infty} \mathbf{u}_{t,\gamma}^* = g_t e^{\bar{f}_t T} \frac{\mathbf{x}_T - e^{\bar{f}_t T} \mathbf{x}_t - \mathbf{m} e^{\bar{f}_t T} \bar{h}_{t:T}}{e^{2\bar{f}_t T} \bar{g}_{t:T}^2}. \quad (12)$$

Now we calculate the transition probability $p(\mathbf{x}_T | \mathbf{x}_t)$ and related h function $\mathbf{h}(\mathbf{x}_t, t, \mathbf{x}_T, T)$.

Consider $F(\mathbf{x}_t, t) = \mathbf{x}_t e^{-\bar{f}_t}$, according to the Ito differential formula, we get:

$$dF = -f_t \mathbf{x}_t e^{-\bar{f}_t} dt + e^{-\bar{f}_t} d\mathbf{x}_t \quad (35)$$

$$\Rightarrow dF = -f_t \mathbf{x}_t e^{-\bar{f}_t} dt + e^{-\bar{f}_t} \left((f_t \mathbf{x}_t + h_t \mathbf{m}) dt + g_t d\mathbf{w}_t \right), \quad (36)$$

$$\Rightarrow dF = h_t e^{-\bar{f}_t} \mathbf{m} dt + e^{-\bar{f}_t} g_t d\mathbf{w}_t, \quad (37)$$

$$\Rightarrow \mathbf{x}_T e^{-\bar{f}_T} - \mathbf{x}_t e^{-\bar{f}_t} = \mathbf{m} \bar{h}_{t:T} + \int_t^T e^{-\bar{f}_z} g_z d\mathbf{w}_z, \quad (38)$$

$$\Rightarrow \mathbf{x}_T \sim N \left(e^{\bar{f}_t T} \mathbf{x}_t + \mathbf{m} e^{\bar{f}_t T} \bar{h}_{t:T}, e^{2\bar{f}_t T} \bar{g}_{t:T}^2 \mathbf{I} \right), \quad (39)$$

$$\Rightarrow \nabla_{\mathbf{x}_t} \log p(\mathbf{x}_T | \mathbf{x}_t) = -\nabla_{\mathbf{x}_t} \frac{(\mathbf{x}_T - e^{\bar{f}_t T} \mathbf{x}_t - \mathbf{m} e^{\bar{f}_t T} \bar{h}_{t:T})^2}{2e^{2\bar{f}_t T} \bar{g}_{t:T}^2} = \frac{e^{\bar{f}_t T} (\mathbf{x}_T - e^{\bar{f}_t T} \mathbf{x}_t - \mathbf{m} e^{\bar{f}_t T} \bar{h}_{t:T})}{e^{2\bar{f}_t T} \bar{g}_{t:T}^2}, \quad (40)$$

$$\Rightarrow \mathbf{u}_{t,\infty}^* = g_t e^{\bar{f}_t T} \frac{\mathbf{x}_T - e^{\bar{f}_t T} \mathbf{x}_t - \mathbf{m} e^{\bar{f}_t T} \bar{h}_{t:T}}{e^{2\bar{f}_t T} \bar{g}_{t:T}^2} = g_t \nabla_{\mathbf{x}_t} \log p(\mathbf{x}_T | \mathbf{x}_t) = g_t \mathbf{h}(\mathbf{x}_t, t, \mathbf{x}_T, T). \quad (41)$$

The forward SDEs obtained through SOC and Doob's h-transform are both formed as

$$d\mathbf{x}_t = \left(f_t \mathbf{x}_t + h_t \mathbf{m} + g_t^2 \frac{e^{\bar{f}_t T} (\mathbf{x}_T - e^{\bar{f}_t T} \mathbf{x}_t - \mathbf{m} e^{\bar{f}_t T} \bar{h}_{t:T})}{e^{2\bar{f}_t T} \bar{g}_{t:T}^2} \right) dt + g_t d\mathbf{w}_t, \quad (42)$$

and the both backward SDEs are

$$d\mathbf{x}_t = \left(f_t \mathbf{x}_t + h_t \mathbf{m} + g_t^2 \frac{e^{\bar{f}_t T} (\mathbf{x}_T - e^{\bar{f}_t T} \mathbf{x}_t - \mathbf{m} e^{\bar{f}_t T} \bar{h}_{t:T})}{e^{2\bar{f}_t T} \bar{g}_{t:T}^2} - g_t^2 \nabla_{\mathbf{x}_t} p(\mathbf{x}_t | \mathbf{x}_T) \right) dt + g_t d\mathbf{w}_t, \quad (43)$$

which concludes the proof of the Theorem 4.2. \square

A.3 DERIVATION OF THE TRANSITION PROBABILITY (16)

Suppose $\bar{\mu}_{t,\gamma}$ and $\bar{\sigma}_t'$ denote the mean value and variance of the transition probability $p(\mathbf{x}_t | x_0, x_T)$, then

$$\begin{aligned} p(\mathbf{x}_t | x_0, x_T) &= \mathcal{N}(\bar{\mu}_{t,\gamma}, \bar{\sigma}_t'^2 \mathbf{I}), \\ \bar{\mu}_{t,\gamma} &= e^{\bar{f}_t} \left(\frac{d_{t,\gamma}}{d_{0,\gamma}} x_0 + \frac{e^{\bar{f}_t} \bar{g}_t^2}{d_{0,\gamma}} x_T + \left(\bar{h}_t - \frac{e^{2\bar{f}_t} \bar{h}_T \bar{g}_t^2}{d_{0,\gamma}} \right) \mathbf{m} \right), \\ \bar{\sigma}_{s:t}^2 &= e^{2\bar{f}_t} \bar{g}_{s:t}^2, \quad \bar{\sigma}_t'^2 = \frac{\bar{\sigma}_t^2 \bar{\sigma}_{t:T}^2}{\bar{\sigma}_T^2}. \end{aligned} \quad (16)$$

Proof. Since $\bar{\mu}_{t,\gamma}$ remains the same as the closed-form relationship (13), we would focus on how to obtain $\bar{\sigma}_{s:t}^2$ and $\bar{\sigma}_t'^2$.

In Equation (35) of Theorem 4.2, we've obtained:

$$\begin{aligned} p(\mathbf{x}_t | \mathbf{x}_s) &\sim N \left(e^{\bar{f}_{s:t}} \mathbf{x}_s + \mathbf{m} e^{\bar{f}_t} \bar{h}_{s:t}, e^{2\bar{f}_t} \bar{g}_{s:t}^2 \mathbf{I} \right), \\ &\sim N \left(e^{\bar{f}_{s:t}} \mathbf{x}_s + \mathbf{m} e^{\bar{f}_t} \bar{h}_{s:t}, \bar{\sigma}_{s:t}^2 \mathbf{I} \right). \end{aligned} \quad (44)$$

Take $\bar{\sigma}_{s:t}^2 = e^{2\bar{f}_t} \bar{g}_{s:t}^2$ as the coefficient of the noise term, then, through Bayes' formula,

$$\begin{aligned} p(\mathbf{x}_t | x_0, x_T) &= \frac{p(x_T | \mathbf{x}_t, x_0)p(\mathbf{x}_t | x_0)}{p(x_T | x_0)} = \frac{p(x_T | \mathbf{x}_t)p(\mathbf{x}_t | x_0)}{p(x_T | x_0)} \\ \Rightarrow \bar{\sigma}_t'^2 &= \frac{\bar{\sigma}_t^2 \bar{\sigma}_{t:T}^2}{\bar{\sigma}_T^2}, \end{aligned}$$

which concludes the derivation of the the transition probability (16). \square

A.4 DERIVATION OF THE TRAINING OBJECTIVE (17)

Denote $a_{t,\gamma} = e^{\bar{f}_t} d_{t,\gamma}$, assuming $\boldsymbol{\mu}_{t-1,\theta}$, $\sigma_{t-1,\theta}^2$ and $\boldsymbol{\mu}_{t-1,\gamma}$, $\sigma_{t-1,\gamma}^2$ are respectively the mean values and variances of $p_\theta(\mathbf{x}_{t-1} | \mathbf{x}_t, x_T)$ and $p(\mathbf{x}_{t-1} | \mathbf{x}_0, \mathbf{x}_t, x_T)$, suppose the score $\nabla_{\mathbf{x}_t} \log p(\mathbf{x}_t | x_T)$ is parameterized as $-\epsilon_\theta(\mathbf{x}_t, x_T, t)/\bar{\sigma}_t'$, the final training objective is as follows,

$$\begin{aligned} \mathcal{L}_\theta &= \mathbb{E}_{t, \mathbf{x}_0, \mathbf{x}_t, \mathbf{x}_T} \left[\frac{1}{2\sigma_{t-1,\theta}^2} \|\boldsymbol{\mu}_{t-1,\theta} - \boldsymbol{\mu}_{t-1,\gamma}\|_1 \right], \\ \boldsymbol{\mu}_{t-1,\theta} &= \mathbf{x}_t - f_t \mathbf{x}_t - h_t \mathbf{m} - g_t \mathbf{u}_{t,\gamma}^* + \frac{g_t^2}{\bar{\sigma}_t'} \epsilon_\theta(\mathbf{x}_t, x_T, t), \\ \boldsymbol{\mu}_{t-1,\gamma} &= \bar{\boldsymbol{\mu}}_{t-1,\gamma} + \frac{\bar{\sigma}_{t-1}^2 a_{t,\gamma}}{\bar{\sigma}_t'^2 a_{t-1,\gamma}} (\mathbf{x}_t - \bar{\boldsymbol{\mu}}_{t,\gamma}), \quad \sigma_{t-1,\theta} = g_t. \end{aligned} \quad (17)$$

Proof. Firstly, as for the training objective (17), according to GOUB Yue et al. (2023):

$$\begin{aligned} \mathbb{E}_{p(\mathbf{x}_0)} [\log p_\theta(\mathbf{x}_0 | x_T)] &\geq \mathbb{E}_{p(\mathbf{x}_0)} \left[\mathbb{E}_{p(\mathbf{x}_1 | \mathbf{x}_0)} [\log p_\theta(\mathbf{x}_0 | \mathbf{x}_1, x_T)] \right. \\ &\quad \left. - \sum_{t=2}^T \mathbb{E}_{p(\mathbf{x}_t | \mathbf{x}_0)} [KL(p(\mathbf{x}_{t-1} | \mathbf{x}_0, \mathbf{x}_t, x_T) || p_\theta(\mathbf{x}_{t-1} | \mathbf{x}_t, x_T))] \right] \\ &= ELBO. \end{aligned} \quad (45)$$

Accordingly,

$$\begin{aligned} &KL(p(\mathbf{x}_{t-1} | \mathbf{x}_0, \mathbf{x}_t, x_T) || p_\theta(\mathbf{x}_{t-1} | \mathbf{x}_t, x_T)) \\ &= \mathbb{E}_{p(\mathbf{x}_{t-1} | \mathbf{x}_0, \mathbf{x}_t, x_T)} \left[\log \frac{\frac{1}{\sqrt{2\pi}\sigma_{t-1}} e^{-(\mathbf{x}_{t-1} - \boldsymbol{\mu}_{t-1,\gamma})^2 / 2\sigma_{t-1}^2}}{\frac{1}{\sqrt{2\pi}\sigma_{\theta,t-1}} e^{-(\mathbf{x}_{t-1} - \boldsymbol{\mu}_{\theta,t-1})^2 / 2\sigma_{\theta,t-1}^2}} \right] \\ &= \mathbb{E}_{p(\mathbf{x}_{t-1} | \mathbf{x}_0, \mathbf{x}_t, x_T)} [\log \sigma_{\theta,t-1} - \log \sigma_{t-1} - (\mathbf{x}_{t-1} - \boldsymbol{\mu}_{t-1,\gamma})^2 / 2\sigma_{t-1}^2 + (\mathbf{x}_{t-1} - \boldsymbol{\mu}_{\theta,t-1})^2 / 2\sigma_{\theta,t-1}^2] \\ &= \log \sigma_{\theta,t-1} - \log \sigma_{t-1} - \frac{1}{2} + \frac{\sigma_{t-1}^2}{2\sigma_{\theta,t-1}^2} + \frac{(\boldsymbol{\mu}_{t-1,\gamma} - \boldsymbol{\mu}_{\theta,t-1})^2}{2\sigma_{\theta,t-1}^2}. \end{aligned} \quad (46)$$

Hence, we ignore some constants and minimizing the negative ELBO, leading to the training objective:

$$\mathcal{L} = \mathbb{E}_{t, \mathbf{x}_0, \mathbf{x}_t, \mathbf{x}_T} \left[\frac{1}{2\sigma_{t-1,\theta}^2} \|\boldsymbol{\mu}_{t-1,\theta} - \boldsymbol{\mu}_{t-1,\gamma}\| \right], \quad (47)$$

Then, as for solving the closed form of $\boldsymbol{\mu}_{t-1,\theta}$, $\sigma_{t-1,\theta}^2$ and $\boldsymbol{\mu}_{t-1,\gamma}$, through Bayes' formula,

$$\begin{aligned} p(\mathbf{x}_{t-1} | x_0, \mathbf{x}_t, x_T) &= \frac{p(\mathbf{x}_t | x_0, \mathbf{x}_{t-1}, x_T)p(\mathbf{x}_{t-1} | \mathbf{x}_0, \mathbf{x}_T)}{p(\mathbf{x}_t | x_0, x_T)} \\ &= \frac{p(\mathbf{x}_t | \mathbf{x}_{t-1}, x_T)p(\mathbf{x}_{t-1} | x_0, \mathbf{x}_T)}{p(\mathbf{x}_t | x_0, x_T)}. \end{aligned} \quad (48)$$

According to Appendix A.3, applying the reparameterization tricks:

$$\begin{aligned}
\mathbf{x}_t &= e^{\bar{f}_t} \left(\frac{\gamma^{-1} + e^{2\bar{f}_T} \bar{g}_{t:T}^2}{\gamma^{-1} + e^{2\bar{f}_T} \bar{g}_T^2} x_0 + \frac{e^{\bar{f}_T} \bar{g}_t^2}{\gamma^{-1} + e^{2\bar{f}_T} \bar{g}_T^2} x_T + \left(\bar{h}_t - \frac{e^{2\bar{f}_T} \bar{h}_T \bar{g}_t^2}{\gamma^{-1} + e^{2\bar{f}_T} \bar{g}_T^2} \right) \mathbf{m} \right) + \bar{\sigma}'_t \epsilon_t \\
&\triangleq a_{t,\gamma} x_0 + b_{t,\gamma} x_T + c_{t,\gamma} \mathbf{m} + \bar{\sigma}'_t \epsilon_t, \\
\mathbf{x}_{t-1} &= e^{\bar{f}_{t-1}} \left(\frac{\gamma^{-1} + e^{2\bar{f}_T} \bar{g}_{t-1:T}^2}{\gamma^{-1} + e^{2\bar{f}_T} \bar{g}_T^2} x_0 + \frac{e^{\bar{f}_T} \bar{g}_{t-1}^2}{\gamma^{-1} + e^{2\bar{f}_T} \bar{g}_T^2} x_T + \left(\bar{h}_{t-1} - \frac{e^{2\bar{f}_T} \bar{h}_T \bar{g}_{t-1}^2}{\gamma^{-1} + e^{2\bar{f}_T} \bar{g}_T^2} \right) \mathbf{m} \right) + \bar{\sigma}'_{t-1} \epsilon_{t-1} \\
&= a_{t-1,\gamma} x_0 + b_{t-1,\gamma} x_T + c_{t-1,\gamma} \mathbf{m} + \bar{\sigma}'_{t-1} \epsilon_{t-1}.
\end{aligned} \tag{49}$$

Therefore, eliminating x_0 to obtain the relationships between \mathbf{x}_t , \mathbf{x}_{t-1} , x_T , \mathbf{m} and noise ϵ ,

$$\Rightarrow \mathbf{x}_t = \frac{a_{t,\gamma}}{a_{t-1,\gamma}} \mathbf{x}_{t-1} + \left(b_{t,\gamma} - b_{t-1,\gamma} \frac{a_{t,\gamma}}{a_{t-1,\gamma}} \right) x_T + \left(c_{t,\gamma} - c_{t-1,\gamma} \frac{a_{t,\gamma}}{a_{t-1,\gamma}} \right) \mathbf{m} + \sqrt{\bar{\sigma}'_t{}^2 - \bar{\sigma}'_{t-1}{}^2 \frac{a_{t,\gamma}^2}{a_{t-1,\gamma}^2}} \epsilon. \tag{50}$$

The mean value $\boldsymbol{\mu}_{t-1,\gamma}$ of $p(\mathbf{x}_{t-1} | x_0, \mathbf{x}_t, x_T)$ can be calculated as:

$$\begin{aligned}
\boldsymbol{\mu}_{t-1,\gamma} &= \frac{\bar{\sigma}'_{t-1}{}^2 \frac{a_{t,\gamma}}{a_{t-1,\gamma}} \left[\mathbf{x}_t - \left(b_{t,\gamma} - b_{t-1,\gamma} \frac{a_{t,\gamma}}{a_{t-1,\gamma}} \right) x_T - \left(c_{t,\gamma} - c_{t-1,\gamma} \frac{a_{t,\gamma}}{a_{t-1,\gamma}} \right) \mathbf{m} \right] + \left(\bar{\sigma}'_t{}^2 - \bar{\sigma}'_{t-1}{}^2 \frac{a_{t,\gamma}^2}{a_{t-1,\gamma}^2} \right) \bar{\boldsymbol{\mu}}_{t-1,\gamma}}{\bar{\sigma}'_t{}^2} \\
&= \bar{\boldsymbol{\mu}}_{t-1,\gamma} - \frac{a_{t,\gamma}^2 \bar{\sigma}'_{t-1}{}^2}{a_{t-1,\gamma}^2 \bar{\sigma}'_t{}^2} \bar{\boldsymbol{\mu}}_{t-1,\gamma} + \frac{a_{t,\gamma} \bar{\sigma}'_{t-1}{}^2}{a_{t-1,\gamma} \bar{\sigma}'_t{}^2} \left[\mathbf{x}_t - \left(b_{t,\gamma} - \frac{a_{t,\gamma} b_{t-1,\gamma}}{a_{t-1,\gamma}} \right) x_T - \left(c_{t,\gamma} - \frac{a_{t,\gamma} c_{t-1,\gamma}}{a_{t-1,\gamma}} \right) \mathbf{m} \right] \\
&= \bar{\boldsymbol{\mu}}_{t-1,\gamma} + \frac{a_{t,\gamma} \bar{\sigma}'_{t-1}{}^2}{a_{t-1,\gamma} \bar{\sigma}'_t{}^2} \mathbf{x}_t - \frac{a_{t,\gamma} \bar{\sigma}'_{t-1}{}^2}{a_{t-1,\gamma} \bar{\sigma}'_t{}^2} \bar{\boldsymbol{\mu}}_{t,\gamma} \\
&= \bar{\boldsymbol{\mu}}_{t-1,\gamma} + \frac{\bar{\sigma}'_{t-1}{}^2 a_{t,\gamma}}{\bar{\sigma}'_t{}^2 a_{t-1,\gamma}} (\mathbf{x}_t - \bar{\boldsymbol{\mu}}_{t,\gamma}).
\end{aligned} \tag{51}$$

with the fact that

$$\bar{\boldsymbol{\mu}}_{t,\gamma} = \frac{a_{t,\gamma}}{a_{t-1,\gamma}} \bar{\boldsymbol{\mu}}_{t-1,\gamma} + \left(b_{t,\gamma} - \frac{a_{t,\gamma} b_{t-1,\gamma}}{a_{t-1,\gamma}} \right) x_T + \left(c_{t,\gamma} - \frac{a_{t,\gamma} c_{t-1,\gamma}}{a_{t-1,\gamma}} \right) \mathbf{m}, \tag{52}$$

which can be easily proved by expanding and comparing the both sides of the equation.

As for $\boldsymbol{\mu}_{\theta,t-1}$ and $\sigma_{t-1,\theta}^2$, parameterized from the SDE (14):

$$\begin{aligned}
\mathbf{x}_{t-1} &= \mathbf{x}_t - \left[f_t \mathbf{x}_t + h_t \mathbf{m} + g_t^2 \frac{x_T - e^{\bar{f}_{t:T}} \mathbf{x}_t - \mathbf{m} e^{\bar{f}_T} \bar{h}_{t:T}}{e^{-\bar{f}_{t:T}} (\gamma^{-1} + e^{2\bar{f}_T} \bar{g}_{t:T}^2)} - g_t^2 \nabla_{\mathbf{x}_t} \log p(\mathbf{x}_t | \mathbf{x}_T) \right] - g_t \epsilon_t \\
&\approx \mathbf{x}_t - \left[f_t \mathbf{x}_t + h_t \mathbf{m} + g_t^2 \frac{x_T - e^{\bar{f}_{t:T}} \mathbf{x}_t - \mathbf{m} e^{\bar{f}_T} \bar{h}_{t:T}}{e^{-\bar{f}_{t:T}} (\gamma^{-1} + e^{2\bar{f}_T} \bar{g}_{t:T}^2)} - \frac{g_t^2}{\bar{\sigma}'_t} \boldsymbol{\epsilon}_\theta(\mathbf{x}_t, x_T, t) \right] - g_t \epsilon_t,
\end{aligned} \tag{53}$$

where $\epsilon_t \sim N(\mathbf{0}, dt\mathbf{I})$.

Hence,

$$\begin{aligned}
\boldsymbol{\mu}_{\theta,t-1} &= \mathbf{x}_t - \left[f_t \mathbf{x}_t + h_t \mathbf{m} + g_t^2 \frac{x_T - e^{\bar{f}_{t:T}} \mathbf{x}_t - \mathbf{m} e^{\bar{f}_T} \bar{h}_{t:T}}{e^{-\bar{f}_{t:T}} (\gamma^{-1} + e^{2\bar{f}_T} \bar{g}_{t:T}^2)} - \frac{g_t^2}{\bar{\sigma}'_t} \boldsymbol{\epsilon}_\theta(\mathbf{x}_t, x_T, t) \right], \\
\sigma_{\theta,t-1} &= g_t,
\end{aligned} \tag{54}$$

which concludes the derivation of the training objective (17). \square

A.5 DERIVATION OF UNIDB-GOU (FORWARD SDE AND MEAN VALUE OF FORWARD TRANSITION (18))

Consider the SOC problem with GOU process (4), the optimally controlled forward SDE and the mean value of forward transition $p(\mathbf{x}_t | x_0, x_T)$ are respectively:

$$d\mathbf{x}_t = \left(\theta_t + \frac{g_t^2 e^{-2\bar{\theta}_{t:T}}}{\gamma^{-1} + \bar{\sigma}_{t:T}^2}\right)(x_T - \mathbf{x}_t)dt + g_t d\mathbf{w}_t, \bar{\boldsymbol{\mu}}_{t,\gamma} = e^{-\bar{\theta}_t} \frac{1 + \gamma \bar{\sigma}_{t:T}^2}{1 + \gamma \bar{\sigma}_T^2} x_0 + (1 - e^{-\bar{\theta}_t} \frac{1 + \gamma \bar{\sigma}_{t:T}^2}{1 + \gamma \bar{\sigma}_T^2}) x_T. \quad (18)$$

Proof. Consider the SOC problem with GOU process (4) in the deterministic form:

$$\begin{aligned} \min_{\mathbf{u}_{t,\gamma}} \int_0^T \frac{1}{2} \|\mathbf{u}_{t,\gamma}\|_2^2 dt + \frac{\gamma}{2} \|\mathbf{x}_T^u - x_T\|_2^2 \\ \text{s.t. } d\mathbf{x}_t = (\theta_t(x_T - \mathbf{x}_t) + g_t \mathbf{u}_{t,\gamma}) dt, \quad \mathbf{x}_0 = x_0 \end{aligned} \quad (55)$$

where the definition of $\boldsymbol{\mu}$ and g_t is the same as GOUB: $\boldsymbol{\mu} = x_T g_t^2 = 2\lambda^2 \theta_t$.

Similarly to the proof of Proposition A.1, according to minimum principle theorem to obtain the following set of differential equations:

$$\frac{d\mathbf{x}_t}{dt} = \nabla_{\mathbf{p}_t} H(\mathbf{x}_t, \mathbf{p}_t, \mathbf{u}_{t,\gamma}^*, t) = \theta_t x_T - \theta_t \mathbf{x}_t - g_t^2 \mathbf{p}_t, \quad (56)$$

$$\frac{d\mathbf{p}_t}{dt} = -\nabla_{\mathbf{x}_t} H(\mathbf{x}_t, \mathbf{p}_t, \mathbf{u}_{t,\gamma}^*, t) = \theta_t \mathbf{p}_t, \quad (57)$$

$$\mathbf{x}_0 = x_0, \quad (58)$$

$$\mathbf{p}_T = \gamma(\mathbf{x}_T - x_T). \quad (59)$$

Solving the equation (57), we have:

$$\begin{aligned} \mathbf{p}_t &= \mathbf{p}_0 e^{\bar{\theta}_t}, \\ \mathbf{p}_T &= \mathbf{p}_0 e^{\bar{\theta}_T}, \end{aligned} \quad (60)$$

Then we solve the equation (56):

$$\begin{aligned} \frac{d\mathbf{x}_t}{dt} &= \theta_t x_T - \theta_t \mathbf{x}_t - g_t^2 \mathbf{p}_t \\ \Rightarrow \frac{d(e^{\bar{\theta}_t} \mathbf{x}_t)}{dt} &= e^{\bar{\theta}_t} \theta_t x_T - e^{\bar{\theta}_t} g_t^2 \mathbf{p}_t, \\ \Rightarrow e^{\bar{\theta}_t} \mathbf{x}_t - \mathbf{x}_0 &= x_T \int_0^t e^{\bar{\theta}_z} \theta_z dz - \mathbf{p}_0 \int_0^t g_z^2 e^{2\bar{\theta}_z} dz, \\ \Rightarrow e^{\bar{\theta}_t} \mathbf{x}_t - x_0 &= x_T (e^{\bar{\theta}_t} - 1) - \lambda^2 \mathbf{p}_0 (e^{2\bar{\theta}_t} - 1). \end{aligned}$$

Hence, we can get:

$$\mathbf{x}_T = e^{-\bar{\theta}_T} x_0 + (1 - e^{-\bar{\theta}_T}) x_T - \lambda^2 \mathbf{p}_T (1 - e^{-2\bar{\theta}_T}), \quad (61)$$

and

$$\mathbf{x}_t = e^{-\bar{\theta}_t} x_0 + (1 - e^{-\bar{\theta}_t}) x_T - \lambda^2 e^{-\bar{\theta}_T} \mathbf{p}_T (e^{\bar{\theta}_t} - e^{-\bar{\theta}_t}). \quad (62)$$

Take the equation (61) into the equation (59) and solve \mathbf{p}_T ,

$$\begin{aligned} \mathbf{p}_T &= \gamma \left(e^{-\bar{\theta}_1} x_0 + (1 - e^{-\bar{\theta}_T}) x_T - \lambda^2 \mathbf{p}_T (1 - e^{-2\bar{\theta}_T}) - x_T \right) \\ \Rightarrow \mathbf{p}_T &= \frac{\gamma e^{-\bar{\theta}_T} (x_0 - x_T)}{1 + \gamma \lambda^2 (1 - e^{-2\bar{\theta}_T})}. \end{aligned}$$

Hence,

$$\begin{aligned}
\mathbf{x}_t &= e^{-\bar{\theta}_t}x_0 + (1 - e^{-\bar{\theta}_t})x_T - \lambda^2 e^{-\bar{\theta}_T} (e^{\bar{\theta}_t} - e^{-\bar{\theta}_t}) \frac{\gamma e^{-\bar{\theta}_T} (x_0 - x_T)}{1 + \gamma \lambda^2 (1 - e^{-2\bar{\theta}_T})} \\
&= \left(e^{-\bar{\theta}_t} - \frac{\gamma \lambda^2 e^{-2\bar{\theta}_T} (e^{\bar{\theta}_t} - e^{-\bar{\theta}_t})}{1 + \gamma \lambda^2 (1 - e^{-2\bar{\theta}_T})} \right) x_0 + \left(1 - e^{-\bar{\theta}_t} + \frac{\gamma \lambda^2 e^{-2\bar{\theta}_T} (e^{\bar{\theta}_t} - e^{-\bar{\theta}_t})}{1 + \gamma \lambda^2 (1 - e^{-2\bar{\theta}_T})} \right) x_T \\
&= \left(e^{-\bar{\theta}_t} \frac{1 + \gamma \lambda^2 (1 - e^{-2\bar{\theta}_T})}{1 + \gamma \lambda^2 (1 - e^{-2\bar{\theta}_T})} \right) x_0 + \left(1 - e^{-\bar{\theta}_t} \frac{1 + \gamma \lambda^2 (1 - e^{-2\bar{\theta}_T})}{1 + \gamma \lambda^2 (1 - e^{-2\bar{\theta}_T})} \right) x_T \\
&= e^{-\bar{\theta}_t} \frac{1 + \gamma \bar{\sigma}_{t:T}^2}{1 + \gamma \bar{\sigma}_T^2} x_0 + \left(1 - e^{-\bar{\theta}_t} \frac{1 + \gamma \bar{\sigma}_{t:T}^2}{1 + \gamma \bar{\sigma}_T^2} \right) x_T,
\end{aligned} \tag{63}$$

which implies

$$\bar{\boldsymbol{\mu}}_{t,\gamma} = e^{-\bar{\theta}_t} \frac{1 + \gamma \bar{\sigma}_{t:T}^2}{1 + \gamma \bar{\sigma}_T^2} x_0 + \left(1 - e^{-\bar{\theta}_t} \frac{1 + \gamma \bar{\sigma}_{t:T}^2}{1 + \gamma \bar{\sigma}_T^2} \right) x_T. \tag{64}$$

Then,

$$\begin{aligned}
\mathbf{u}_{t,\gamma}^* &= -g_t \mathbf{p}_t \\
&= -g_t e^{\bar{\theta}_t} e^{-\bar{\theta}_T} \frac{\gamma e^{-\bar{\theta}_T} (x_0 - x_T)}{1 + \gamma \lambda^2 (1 - e^{-2\bar{\theta}_T})} \\
&= -g_t e^{\bar{\theta}_t} e^{-\bar{\theta}_T} \frac{\gamma e^{-\bar{\theta}_T} (x_0 - x_T)}{1 + \gamma \bar{\sigma}_T^2} \\
&= -g_t e^{\bar{\theta}_t} e^{-\bar{\theta}_T} \frac{\gamma e^{-\bar{\theta}_T} e^{\bar{\theta}_t} (\mathbf{x}_t - x_T)}{1 + \gamma \bar{\sigma}_{t:T}^2} \\
&= g_t \frac{e^{-2\bar{\theta}_t:T} (x_T - \mathbf{x}_t)}{\gamma^{-1} + \bar{\sigma}_{t:T}^2}.
\end{aligned} \tag{65}$$

And the optimally-controlled dynamics can be:

$$d\mathbf{x}_t = \left(\theta_t + g_t^2 \frac{e^{-2\bar{\theta}_t:T}}{\gamma^{-1} + \bar{\sigma}_{t:T}^2} \right) (x_T - \mathbf{x}_t) dt + g_t d\mathbf{w}_t, \tag{66}$$

which concludes the derivation of UniDB-GOU (forward SDE and mean value of forward transition (18)). \square

B IMPLEMENTATION DETAILS

In Image Restoration Tasks (Image 4×Super-resolution, Image Deraining and Image Inpainting), we follow the experiment setting of GOUB Yue et al. (2023): the same noise network which is similar to U-Net structure Chung et al. (2022), steady variance level $\lambda^2 = 30^2/255^2$, coefficient $e^{\bar{\theta}_T} = 0.005$ instead of zero, sampling step number $T = 100$, 128 patch size with 8 batch size when training, Adam optimizer with $\beta_1 = 0.9$ and $\beta_2 = 0.99$ Kingma (2014), 1.2 million total training steps with 10^{-4} initial learning rate and decaying by half at 300, 500, 600, and 700 thousand iterations. With respect to the schedule of θ_t , we choose a flipped version of cosine noise schedule Nichol & Dhariwal (2021); Luo et al. (2023),

$$\theta_t = 1 - \frac{\cos\left(\frac{t/T+s}{1+s} \frac{\pi}{2}\right)^2}{\cos\left(\frac{s}{1+s} \frac{\pi}{2}\right)^2} \tag{67}$$

where $s = 0.008$ to achieve a smooth noise schedule. g_t is determined through $g_t^2 = 2\lambda^2\theta_t$. As for the datasets of the three main experiments, we take 800 images for training and 100 for testing for the DIV2K dataset, 1800 images for training and 100 for testing for the Rain100H dataset, 27000 images for training and 3000 for testing for the CelebA-HQ 256×256 dataset. Our models are trained on a single NVIDIA H20 GPU with 96GB memory for about 2 days.

C ADDITIONAL EXPERIMENTAL RESULTS

Here we will illustrate more experimental results.

Table 3: Qualitative comparison between different bridge models (DDBMs (VE) and DDBMs (VP)) and ours (UniDB-VE and UniDB-VP) on DIV2K and Rain100H datasets.

METHOD	Image 4× Super-Resolution				Image Deraining			
	PSNR↑	SSIM↑	LPIPS↓	FID↓	PSNR↑	SSIM↑	LPIPS↓	FID↓
DDBMs (VE)	23.34	0.4295	0.372	32.28	29.34	0.7654	0.185	43.22
UniDB-VE	23.84	0.4454	0.357	31.29	29.46	0.7671	0.185	42.57
DDBMs (VP)	22.11	0.4059	0.491	48.09	29.58	0.828	0.113	35.46
UniDB-VP	22.42	0.4097	0.486	44.52	30.11	0.8414	0.102	33.17

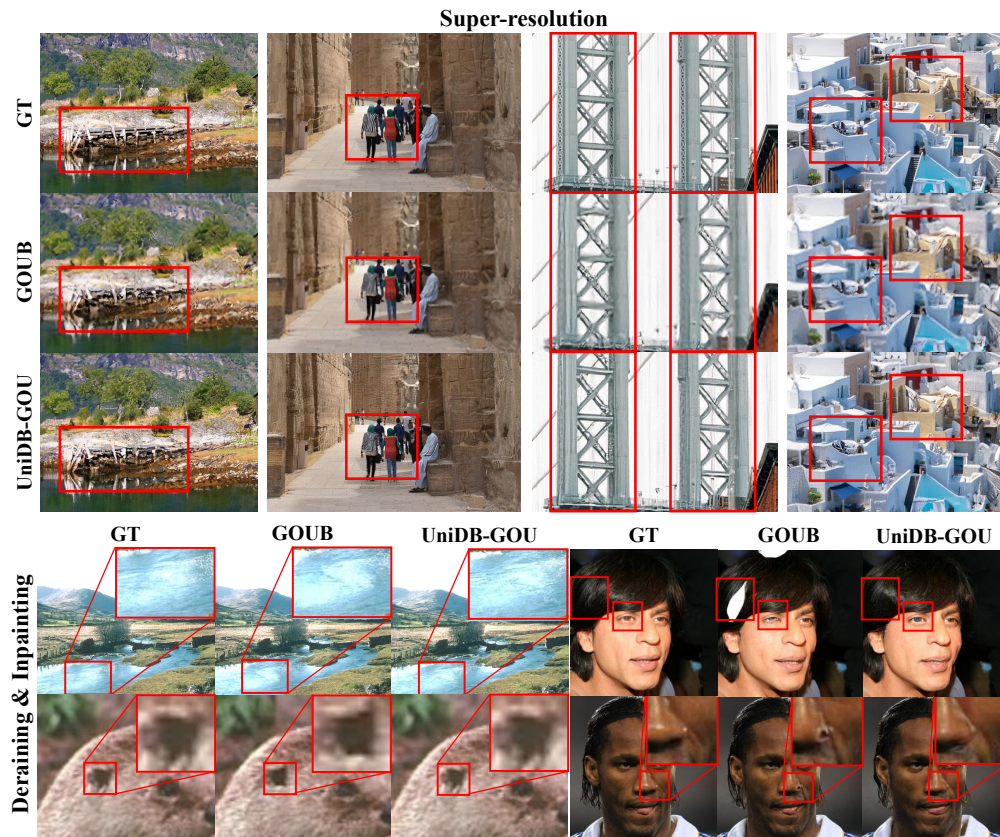


Figure 2: Qualitative comparison of visual results between GOURB (SDE) and UniDB (SDE) on DIV2K, Rain100H, and CelebA-HQ datasets on three tasks with zoomed-in image local regions (UniDB based on GOU process).



Figure 3: Additional visual results on deraining with Rain100H datasets.

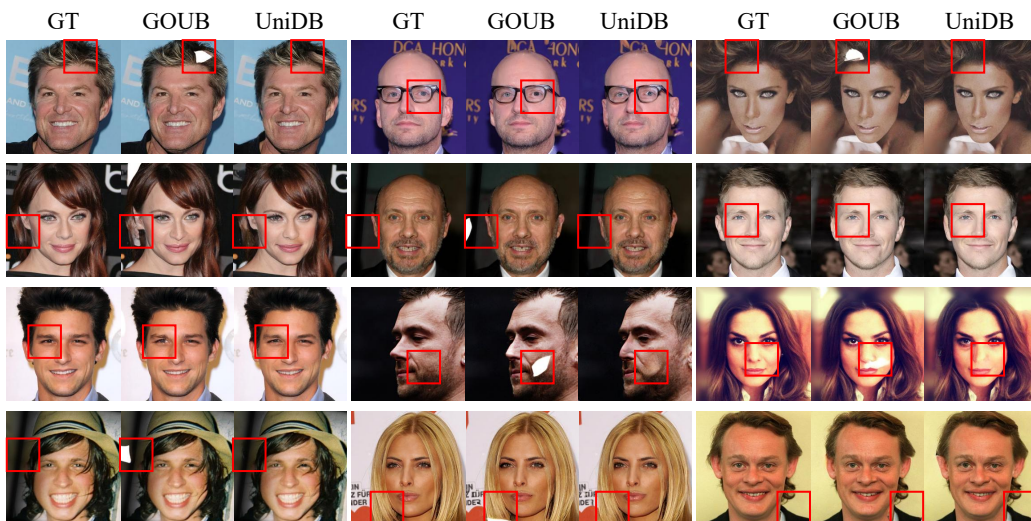


Figure 4: Additional visual results on thin mask inpainting with CelebA-HQ datasets to show our excellence.